# Pointing Control for Low Altitude Triple Cubesat Space Darts

James Armstrong, Craig Casey, Glenn Creamer, Gilbert Dutchover
U.S. Naval Research Laboratory
4555 Overlook Avenue, Washington, DC 20375; (202) 767-1777
jim.armstrong@nrl.navy.mil

## ABSTRACT

Pointing control of cubesats can be quite challenging due to constraints on volume, cost, and complexity of control hardware. Recent achievements and developments in small sensor and actuator designs have enabled the possibility of reasonable pointing performance (a few degrees or better) for a variety of intriguing space experiments. In this paper we describe a simple pointing control design that exploits the aerodynamics associated with the *space dart* geometry of a triple cubesat with deployable solar panels in a low-altitude orbit (< 500 km) to provide passive pitch and yaw stabilization, coupled with a small momentum-biased pitch reaction wheel offering passive yaw and roll stabilization. Augmented active rate damping is provided using a small three-axis magnetometer, three small magnetic torquers, and a model-based B-dot control law. This simple passive/active control system offers experiment pointing capability to less than 5 degrees of nadir without the need for any attitude knowledge.

## INTRODUCTION

The growth of the cubesat community has been quite impressive over the past 6 years[1-4], with a total of 24 cubesats launched since 2003 (another 14 were destroyed in a failed launch attempt). However, with just a few exceptions most cubesats have been built by universities as educational tools, with minimal scientific benefit due to limited real estate and power on a single cubesat bus as well as lack of decent attitude control capability. Recently, growing interest and financing from U.S. government organizations has created more intriguing opportunities for cubesat-class missions. While the majority of cubesat configurations launched have been of the single cubesat class, there have been a few triple cubesats flown, such as QuakeSat[5] (gravity gradient stabilized, though originally designed to track the geomagnetic field), Delfi-C3[6] (slow tumbler), GeneSat[7] (geomagnetic field stabilized), and CanX-2[8] (three-axis controlled to 10 degrees). These triple cubesat buses offer increased real estate and power for payload operations, expanding the scientific and engineering capabilities of these small picosatellites.

Pointing control of cubesats has always been challenging due primarily to volumetric constraints and lack of sufficiently small attitude sensing and control components. Hence, most cubesat control designs rely on general tumbling or, at best, magnetic rate control with large attitude errors. However, as mission opportunities and payload demands increase, accurate pointing control is becoming more critical to the ultimate success of cubesat-class missions. In this paper we describe a simple pointing control design that exploits the aerodynamics associated with the *space dart* geometry of a triple cubesat with deployable solar panels in a low-altitude orbit (< 500 km) to provide passive pitch and yaw stabilization, coupled with a small momentum-biased pitch reaction wheel offering passive yaw and roll stabilization. Augmented active rate damping is provided using a small three-axis magnetometer, three small magnetic torquers, and an International Geomagnetic Reference Field (IGRF) model-based B-dot control law. The triple cubesat space dart seeks to benefit the cubesat community by providing a controlled experiment platform for rapid space validation of small technologies. An overview of the space dart bus is described in the following section, followed by a detailed description and analysis of the passive/active attitude control system, a discussion of the magnetic test program, and a simulation of expected control performance.

## TRIPLE CUBESAT SPACE DART OVERVIEW

The triple cubesat space dart, illustrated in its deployed state in Figure 1, consists of a stack of three standard-sized cubesats and four deployable solar panels. The space dart is jointly developed by the U.S. Naval Research Laboratory (NRL) and its industry partner Pumpkin Space Systems™. The objective of the NRL space dart mission is to verify the functionality and performance of several miniature technologies, specifically an IntelliTech Microsystem Inc. IMI-100 Attitude Determination and Control System (ADACS), a PNI Corp. MicroMag 3 magnetometer, a Clyde-Space Ltd. deployable Electrical Power System, and a

Pumpkin Space Systems™ 3X Cubesat bus design and pluggable command & data handling module architecture. The space dart size is approximately 10 x 10 x 35 cm with an approximate mass of 4.5 kg, and fits into a standard P-POD cubesat dispenser[9] with the solar panels folded down. The deployed configuration allows for passive aerodynamic pitch and yaw control by exploiting the axial symmetry of the four deployed solar panels. Since the deployable solar panels will not allow for an external payload while stored in a P-POD dispenser, any deployable payload must be stowed internally and deployed after release of the solar panels.
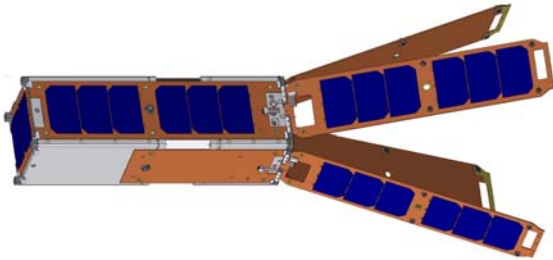


**Figure 1: Triple Cubesat Space Dart Configuration**

The space dart attitude control hardware consists of the IMI-100 ADACS unit and the MicroMag 3 magnetometer. The IMI-100, shown in Figure 2, is a hermetically sealed single cubesat-sized controller capable of providing 3-axis control for a variety of cubesat missions. The unit houses three miniature reaction wheels, three magnetic torque coils, and a processor board capable of calculating attitude, orbit state vectors, and IGRF model vectors. The specifications for the IMI-100 are listed in Table 1. For the space dart configuration in a low-altitude orbit, it is shown in the following section that only one wheel is required to perform payload pointing, with no attitude knowledge necessary.



**Figure 2: IMI-100 ADACS**

**Table 1: IMI-100 Specifications**

| | |
|---|---|
| Reaction Wheel Momentum Storage | 1.1 mNms |
| Maximum Torque | 0.635 mNm |
| Torque Rod Strength | 0.1 A-m$^2$ coils |
| Dimensions | 10 cm x 10 cm x 7.87 cm |
| Weight | 0.907 kg |
| Operating Temperature | -40ºC to +80ºC |
| Vibration | > 10 g-rms |
| Radiation | 30 krad |
| Power Supply | 12 VDC @ 200 mA (typical) |
| Telemetry Rate | 1 Hz |
| Command Process Rate | 4 Hz |

The MicroMag 3 magnetometer, shown circled in red in Figure 3, is integrated onto a circuit board that provides the electrical and communications interface to the IMI-100 unit. The magnetometer measures the local geomagnetic field, providing the necessary sensor data (along with the IGRF vector) for the B-dot control law described in the following section. The specifications for the MicroMag 3 magnetometer are listed in Table 2.



**Figure 3: MicroMag 3 Magnetometer (in red)**

**Table 2: MicroMag 3 Specifications**

| | |
|---|---|
| Measurement Range | ±1100 mT (±11 Gauss) |
| Resolution | ±015 mT (±0.00015 Gauss) |
| Mass | 0.0028 kg |
| Dimensions | 2.54 cm x 2.54 cm x 1.9 cm |
| Operating Temperature | -20ºC to 70ºC |
| Power | < 500 mA (typical) |
| Sample Rate | Up to 2000 samples/sec |

In addition to its aerodynamic characteristics, the space dart configuration also has obvious advantages for power generation. With large deployment angles the power generation can almost be doubled compared to a standard triple cubesat. Furthermore, the higher power capability allows for more real estate availability on the nadir face for payload deployment and viewing. For

power control, opposing panels are coupled into five battery charge regulators (BCR). Each BCR is capable of providing 8 Watts from its two arrays into the batteries. The power generation out of the solar arrays over a typical three-orbit timeframe is shown in Figure 4, where it is observed that peak levels of 15 W are achievable and the daylight orbit-average is about 9 W.
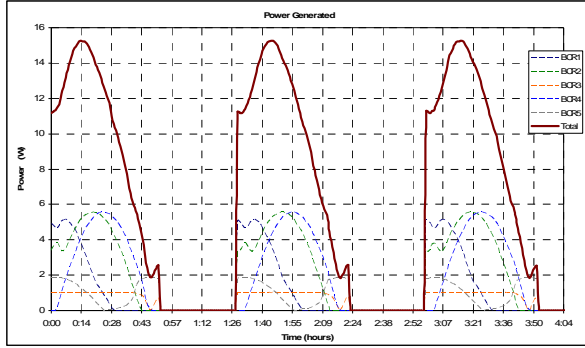


**Figure 4: Typical Space Dart Power Generation**

## SPACE DART POINTING CONTROL LOGIC

The IMI-100 ADACS generally offers 3-axis attitude control capability for a variety of mission orbits. However, for very low orbit altitudes (less than about 400 km) momentum saturation of the small IMI-100 reaction wheels can frequently occur due to aerodynamic disturbances, causing potentially large pointing errors. Additionally, general 3-axis attitude control requires utilization of attitude sensors, such as Sun sensors or Earth sensors, to complement the magnetometer measurements. While simple Sun sensors are readily available, they offer no information during eclipse periods, and small low-cost Earth sensors are still at a relatively low technology readiness level.

To greatly simplify the attitude control system, the space dart pointing controller consists of a combination of passive attitude stabilization and active rate damping control to align the body frame with the orbit frame, without the need for any attitude knowledge capability. Passive attitude stabilization stems from two sources: aerodynamic pitch/yaw stabilization from the solar panels and dynamic roll/yaw stabilization from the reaction wheel. Active inertial rate damping is achieved using the magnetometer, the three magnetic torquers, and the IGRF geomagnetic field model.

*Passive Attitude Stabilization*

As shown in the planar depiction of Figure 5, the space dart solar panels provide ideal surfaces for passive aerodynamic stabilization of both yaw and pitch motion of the body frame *B* relative to the local orbit frame *O*

(rotating at circular orbit rate $\omega_o$ ). For a small pitch error $\theta$ and a panel angle $\gamma < 90$ degrees, it can be shown that the combined restoring torque due to both accommodating and reflective aerodynamic forces impinging on surfaces 1 through 4 can be approximated by

$$u_{aero} = -\frac{1}{18}\rho V^2 C_D L^2 g(\gamma)\theta = -k_a\theta \qquad (1)$$

$$g(\gamma) = \sigma\left[L(\cos\gamma + 6\cos\gamma\sin\gamma - \tfrac{1}{2}) + D(6\sin\gamma + 1)\right]$$
$$+12(1-\sigma)\left[\tfrac{1}{2}L(\cos\gamma + \tfrac{1}{3}\cos\gamma\sin\gamma - \tfrac{1}{2}) + D(\cos^2\gamma + \tfrac{1}{2})\right]$$

where $\rho$ is the local air density, V is the spacecraft velocity, $C_D$ is the panel drag coefficient (typically equal to 2 for flat surfaces), and $\sigma$ is the airflow accommodation factor ($\sigma = 1$ is full surface accommodation, $\sigma = 0$ is full surface reflection)[10]. The effects of airflow obstructions from one surface onto another are neglected in Equation (1). It should also be noted that Equation (1) is valid only for $\theta < \gamma$, since no airflow impingement would occur on surface 4 otherwise. For most practical geometries D will be positive, resulting in a negative-valued (restoring) torque. Due to axisymmetry of the space dart, the same stable restoring torque is generated under small yaw motion. It can also be shown that the equilibrium point $\theta = 0$ is aerodynamically stable as long as the panel angle exceeds the solution to the transcendental equation

$$6[L\cos\gamma + 2D]\sin\gamma = L - D \qquad (2)$$

which, for small panel angles, becomes

$$\gamma > \frac{L-D}{6(L+2D)} \qquad (3)$$

ensuring that the center of pressure, CP, is located behind the center of mass, CM, relative to the airflow.
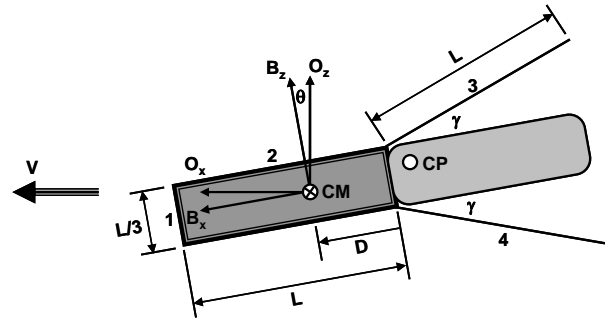


**Figure 5: Planar Depiction of Space Dart Geometry**

---

The pitch reaction wheel offers additional passive dynamic stabilization of both the yaw and roll motion of the body frame relative to the orbit frame. For a small yaw error $\psi$ and a small roll error $\phi$, the wheel momentum $h_w$ provides the well-known restoring torques $h_w \omega_o \psi$ and $h_w \omega_o \phi$, as well as gyric coupling torques $h_w \dot{\psi}$ and $h_w \dot{\phi}$.

### Active Magnetic Rate Damping

A variation of the well-known B-dot magnetic rate damping law is implemented on the space dart using the $6^{th}$-degree IGRF geomagnetic field model residing on the IMI-100. The classical B-dot law removes the body rates relative to the rate of change of the field, rather than relative to inertial space. Since the space dart has no inherent aerodynamic roll stiffness and very little dynamic roll stiffness from the reaction wheel ( $h_w = 0.001$ N-m-s), the resulting periodic roll motion can exceed 10 degrees under this classical B-dot control law. Therefore, we implement an approximate modified B-dot law using the known spacecraft position from the IMI-100 orbit propagator and the IGRF model of the field at that position. The exact relation between the derivative of the field vector **B** with respect to a reference inertial frame $I$ and the derivative of **B** with respect to the body frame $B$ is

$$\left(\frac{d\mathbf{B}}{dt}\right)^I = \left(\frac{d\mathbf{B}}{dt}\right)^B + \boldsymbol{\omega}_{B/I} \times \mathbf{B} \qquad (4)$$

where $\boldsymbol{\omega}_{B/I}$ is the inertial body rate vector. The expression on the left hand side represents the time derivative of the value obtained from the field model, which is known in the inertial frame. To express this relation in a consistent coordinate frame we must transform the left hand side vector to the body frame. Re-arranging the expression and writing in matrix form leads to

$$
\begin{aligned}
[\boldsymbol{\omega}_{B/I}]^x \{\mathbf{B}\} &= [\mathbf{C}_{B/I}]\left(\left(\frac{d\{\mathbf{B}\}}{dt}\right)^I - \left(\frac{d\{\mathbf{B}\}}{dt}\right)^B\right) \\
&= [\mathbf{C}_{B/O}][\mathbf{C}_{O/I}]\left(\left(\frac{d\{\mathbf{B}\}}{dt}\right)^I - \left(\frac{d\{\mathbf{B}\}}{dt}\right)^B\right)
\end{aligned} \qquad (5)
$$

where $[\mathbf{C}_{B/I}]$ is the direction cosine matrix relating the inertial frame to the body frame, $[\mathbf{C}_{B/O}]$ is the direction cosine matrix relating the orbit frame to the body frame, $[\mathbf{C}_{O/I}]$ is the direction cosine matrix relating the inertial frame to the orbit frame (which is determined from the on-board orbit state vector), and

$[\ ]^x$ is the skew-symmetric operator. However, since we are not determining the attitude of the body frame we make the following assumptions based on the fact that we spin the reaction wheel up upon release from the cubesat launch dispenser:

1.  If the initial tip-off rates are large, the first term on the right hand side of Equation (5) will be small compared to the second term and, therefore, negligible. This is the common assumption inherent in the classical B-dot law.
2.  After a brief period of time (perhaps a few orbits), passive aerodynamic and dynamic stability coupled with the active B-dot law will sufficiently remove the majority of rates and attitude errors relative to the local orbit frame such that any resulting errors (primarily in roll due to its weak passive stiffness), coupled with the slow derivative of **B** with respect to the inertial frame, will be negligible. Therefore, the direction cosine matrix $[\mathbf{C}_{B/O}]$ in Equation (5) can be approximated to first-order as the identity matrix at that time.

With these assumptions in mind, the approximate B-dot law we implement for the space dart becomes

$$\{\mathbf{M}\} = k\left(\frac{d([\mathbf{C}_{O/I}]\{\mathbf{B}\}^I - \{\mathbf{B}\}^B)}{dt}\right) \qquad (6)$$

where $\{\mathbf{M}\}$ is the control dipole vector and k is a scalar gain. This simple control law, coupled with the inherent passive control, approximately removes the inertial body rates and aligns the body frame with the orbit frame, without the need for any attitude determination. Hence, an experiment payload aligned with the body negative z-axis (as defined in Figure 5) will continuously look towards the Earth. In the following section we show that, under simplifying practical assumptions, the only stable equilibrium point has the positive wheel momentum direction aligned with the positive orbit angular momentum direction, such that the space dart cannot stabilize in a 180-degree inverted roll orientation.

### Local Pointing Control Stability

Implementation of the modified B-dot law of Equation (6), coupled with the passive aerodynamic and dynamic stiffness associated with the momentum biased space dart, naturally tends to align the space dart longitudinal axis with the local orbital velocity direction and the wheel axis with the orbit normal direction from any arbitrary initial orbit injection state, as long as the wheel momentum is not so large as to overwhelm the

aerodynamic loads. However, in general the wheel could possibly align itself along either the positive or negative orbit momentum direction, with the latter resulting in dire consequences for Earth-viewing payloads. In the following, we show that under some practical assumptions the only stable roll equilibrium point has the positive wheel momentum direction aligned to the positive orbit momentum direction, guaranteeing proper Earth pointing.

To investigate the stability of the equilibrium point $\psi = \theta = \phi = 0$, we start with the approximate equations of motion governing small departure from that point. Here we assume that the aerodynamic stiffness is represented mathematically by the positive-valued linear spring constant $k_a$, and the magnetic inertial rate damping is represented mathematically by the positive-valued linear damping constant $k_m$. The resulting linearized equations of motion for pitch and coupled roll/yaw under aerodynamic, magnetic, and gravity gradient torques becomes

$$I_t \ddot{\theta} + k_m \dot{\theta} + [k_a + 3(I_l - I_t)\omega_o^2]\theta = 0 \qquad (7a)$$

$$\begin{bmatrix} I_l & 0 \\ 0 & I_t \end{bmatrix}\begin{Bmatrix} \ddot{\phi} \\ \ddot{\psi} \end{Bmatrix} + \begin{bmatrix} k_m & I_l\omega_o - h_w \\ h_w - I_l\omega_o & k_m \end{bmatrix}\begin{Bmatrix} \dot{\phi} \\ \dot{\psi} \end{Bmatrix}$$
$$+ \begin{bmatrix} h_w\omega_o & k_m\omega_o \\ -k_m\omega_o & (I_t - I_l)\omega_o^2 + h_w\omega_o + k_a \end{bmatrix}\begin{Bmatrix} \phi \\ \psi \end{Bmatrix} = \begin{Bmatrix} 0 \\ 0 \end{Bmatrix} \qquad (7b)$$

where $I_t$ and $I_l$ are the transverse and longitudinal inertias for the approximate axisymmetric body, with $I_t \gg I_l$. It is clear from the pitch equation, as well as from Figure 5, that the gravity gradient torque is de-stabilizing. However, upon comparing typical numerical values for the aerodynamic stiffness with the gravity gradient stiffness it is observed that $k_a$ is the dominant stiffness term for orbit altitudes below about 500 km as long as the panel angle $\gamma$ is sufficiently large. Furthermore, upon comparing the wheel momentum value for the IMI-100 with the bus gyric stiffness it is observed that $h_w \gg I_l\omega_o$. Therefore, for many practical applications the linearized equations of motion can be approximated as

$$I_t \ddot{\theta} + k_m \dot{\theta} + k_a\theta = 0 \qquad (8a)$$

$$\begin{bmatrix} I_l & 0 \\ 0 & I_t \end{bmatrix}\begin{Bmatrix} \ddot{\phi} \\ \ddot{\psi} \end{Bmatrix} + \begin{bmatrix} k_m & -h_w \\ h_w & k_m \end{bmatrix}\begin{Bmatrix} \dot{\phi} \\ \dot{\psi} \end{Bmatrix}$$
$$+ \begin{bmatrix} h_w\omega_o & k_m\omega_o \\ -k_m\omega_o & I_t\omega_o^2 + h_w\omega_o + k_a \end{bmatrix}\begin{Bmatrix} \phi \\ \psi \end{Bmatrix} = \begin{Bmatrix} 0 \\ 0 \end{Bmatrix} \qquad (8b)$$

where it becomes clear that the uncoupled pitch motion is asymptotically stable to the origin. To investigate the stability of the coupled roll/yaw motion we consider the associated characteristic equation

$$s^4 + a_1 s^3 + a_2 s^2 + a_3 s + a_4 = 0$$

$$a_1 = \frac{k_m(I_t + I_l)}{I_t I_l} \approx \frac{k_m}{I_l}$$

$$a_2 = \frac{I_l(I_t\omega_o^2 + h_w\omega_o + k_a) + I_t h_w\omega_o + k_m^2 + h_w^2}{I_t I_l}$$

$$\approx \frac{I_l k_a + I_t h_w\omega_o + h_w^2}{I_t I_l} \qquad (9)$$

$$a_3 = \frac{k_m(I_t\omega_o^2 + k_a)}{I_t I_l} \approx \frac{k_m k_a}{I_t I_l}$$

$$a_4 = \frac{h_w\omega_o(I_t\omega_o^2 + h_w\omega_o + k_a) + k_m^2\omega_o^2}{I_t I_l}$$

$$\approx \frac{h_w\omega_o k_a}{I_t I_l}$$

where, once again, we have made relative order of magnitude approximations to neglect the insignificant terms. From a Routh-Hurwitz stability analysis we know that each of the four coefficients must have the same sign. Since $a_1$ and $a_3$ are positive by definition, then $a_4$ must also be positive, requiring $h_w$ to have the same sign (direction) as the orbit rate. Additionally, it can be shown that the inequality $a_1(a_2 a_3 - a_1 a_4) - a_3^2 > 0$ necessary for asymptotic stability is automatically satisfied. Therefore, the coupled roll/yaw motion is asymptotically stable to the origin as long as the wheel momentum is in the same direction as the orbit momentum and, consequently, the inverted roll orientation characterized by the wheel momentum opposing the orbit momentum (equivalent to $\phi = 180$ degrees) is an unstable equilibrium point. Hence, under the assumptions outlined throughout this section, the space dart will automatically align its body frame with the orbit frame from any arbitrary initial dynamic state once wheel momentum bias is achieved.

## SPACE DART MAGNETIC TESTING

While the space dart configuration is ideal for exploiting passive aerodynamic drag to assist with active magnetic rate damping, magnetic disturbance torques originating from the spacecraft residual dipole can still have a negative impact on control performance. In order to reduce this effect, the residual dipole must be reduced sufficiently such that the resulting disturbance torques are well below the active torque capability of the magnetic coils. The IMI-100 torque coils have a maximum capability of 0.1 A-m$^2$; however, under pulse width modulation the effective dipole capability is reduced to 0.0374 A-m$^2$. Therefore, a design goal of less than 0.01 A-m$^2$ for the residual spacecraft dipole is imposed. In order to achieve this tight requirement, a magnetic test program is required to measure the powered spacecraft dipole and balance to the design level, if necessary.

Magnetic balancing of a test article generally consists of four primary steps. The first step is to measure the magnetic field of the test facility mounting fixture without the test article attached. The second step is to measure the magnetic field of the test article attached to the mounting fixture, normally with everything power on to emulate the nominal on-orbit configuration. The field obtained from the first step is then subtracted from the field measured with the test article in place. The third step, if necessary, is to place a permanent magnet in a specific orientation on the spacecraft in order to counteract the residual magnetic dipole derived from step 2. The last step is to verify that the permanent magnet is selected and oriented correctly by measuring the magnetic dipole of the balanced spacecraft and confirming that it meets the requirement. Multiple iterations of magnet selection, placement, and verification may be required in order to achieve the desired goal.

In order to measure the magnetic dipole of the NRL space dart, the Helmholtz coil at NASA Goddard's Spacecraft Magnetic Test Facility is used. The Helmholtz coil eliminates the effect of the Earth's magnetic field on the measurements. Four 3-axis magnetometers are located at various stations within the Helmholtz coil in order to obtain multiple field readings for derivation of the spacecraft magnetic dipole. During a test, the spacecraft is rotated 360$^0$ while the facility magnetometers read the magnetic field at 1 degree increments, allowing sufficient derivation of the three-axis dipole vector. The Goddard facility is capable of determining residual dipoles below 0.01 A-m$^2$.

A picture of NRL's space dart attached to its mounting fixture inside Goddard's magnetic test facility is shown in Figure 6. Based on the facility magnetometer readings, an average spacecraft dipole of about 0.009 A-m$^2$ was calculated in full powered-up mode. Since this value is about 10% lower than the design goal of 0.01 A-m$^2$, no magnetic balancing was necessary.
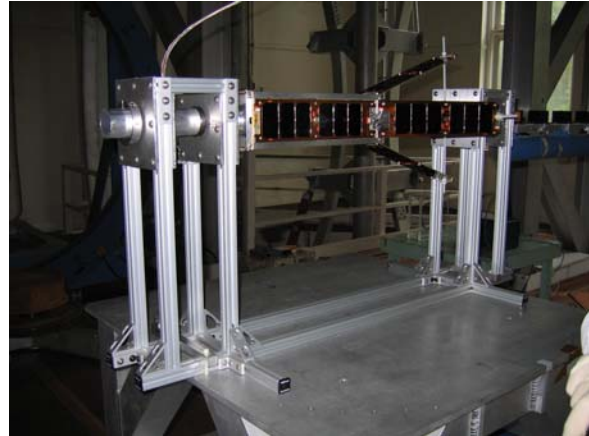


**Figure 6: The NRL Space Dart in NASA Goddard's Spacecraft Magnetic Test Facility**

## SPACE DART POINTING CONTROL PERFORMANCE

In this section we provide two examples of the simple space dart pointing controller described previously. The goal is to point an experiment payload, whose viewing axis is aligned with the spacecraft negative z-axis, towards the Earth from an initial launch dispenser tip-off state. The space dart physical characteristics and controller parameters, as well as the orbit elements, are listed in Table 3. In case 1, the orbit altitude is 300 km and the panel angle is 20 degrees, whereas in case 2 the orbit altitude is 500 km and the panel angle is 45 degrees. We utilize a 6$^{th}$-degree geomagnetic reference field model (as is available on the IMI-100) and a magnetometer modeled with random 1-sigma noise of 150 nanoTesla per axis, which is smoothed using a digital low-pass filter with a roll-off frequency of about 0.04 Hz. The controller is insensitive to magnetometer biases, as a natural consequence of the B-dot law. The airflow density is assumed to be consistent with average solar activity conditions. Using initial dispenser tip-off rates of 3 degrees/second about each axis, the resulting spacecraft heading angles and Earth-pointing angles are shown in Figures 7 and 8 for both cases. Reasonable pointing performance (< 5 degrees) is achieved within about four orbits for case 1 and five orbits for case 2. The magnitudes of the aerodynamic and gravity gradient torques are shown in Figures 9 and 10 for both cases, highlighting the sensitivity of the two disturbance

sources to altitude. For the lower altitude case, the aerodynamic torques exceed the gravity gradient torques by over an order of magnitude, offering stiff aerodynamically-stabilized control performance. In contrast, the higher altitude case reveals that the aerodynamic torques are only slightly larger than the gravity gradient torques, with greatly reduced aerodynamic stiffness. At altitudes much beyond 500 km, it is expected that the aerodynamic torques acting on the space dart would be insufficient for maintaining good control performance.

**Table 3: Space Dart Parameters**

| Parameter | Description | Value |
|-----------|-------------|-------|
| L | Main Bus Length | 35 cm |
| D | CM Location | 6 cm |
| $\gamma$ | Solar Panel Angle | 20 deg (case 1)<br>45 deg (case 2) |
| $\sigma$ | Airflow Accommodation Factor | 1 |
| $\rho$ | Airflow Density | 3.0e-11 kg/m$^3$ (case 1)<br>0.8e-12 kg/m$^3$ (case 2) |
| $C_D$ | Drag Coefficient | 2 |
| k | B-dot Gain | 200 A-m$^2$-s/Tesla |
| $M_{max}$ | Maximum Dipole | 0.05 A-m$^2$ |
| $h_w$ | Wheel Momentum | 0.0009 N-m-s |
| $I_t$ | Transverse Spacecraft Inertia | 0.29 kg-m$^2$ |
| $I_l$ | Longitudinal Spacecraft Inertia | 0.016 kg-m$^2$ |
| h | Orbit Altitude | 300 km (case 1)<br>500 km (case 2) |
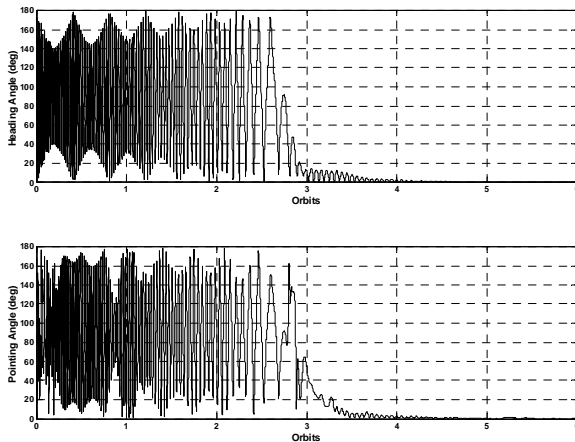


**Figure 7: Control Performance for the 300 km Orbit**
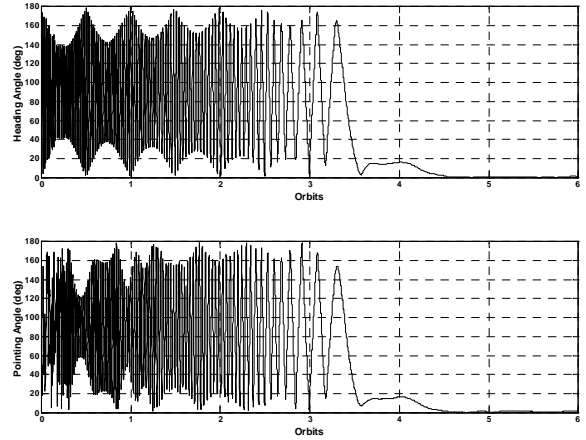


**Figure 8: Control Performance for the 500 km Orbit**
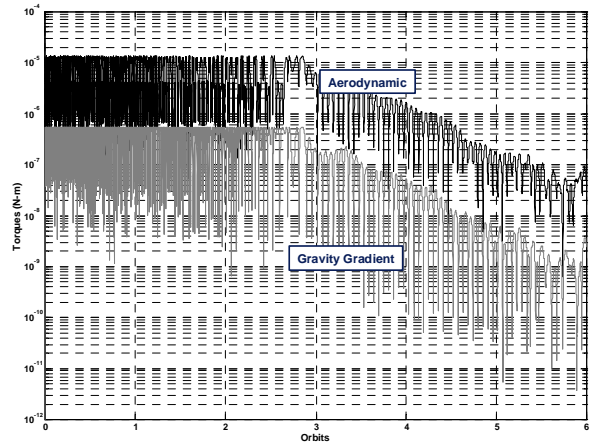


**Figure 9: Aerodynamic and Gravity Gradient Torques for the 300 km Orbit**
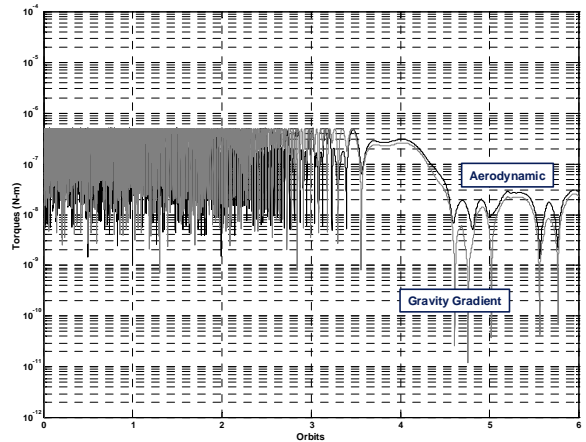


**Figure 10: Aerodynamic and Gravity Gradient Torques for the 500 km Orbit**

## CONCLUSIONS

The triple cubesat space dart configuration offers many intriguing advantages over standard single cubesats and triple cubesat stacks. Payload real estate is approximately tripled over single cubesats, and available power is increased nearly sixfold over single cubesats and twofold over triple stacks, with a daylight average approaching 9 W and a peak approaching 15 W. As described in this paper, another advantage for low-altitude orbits is the exploitation of aerodynamic characteristics of the space dart to eliminate any need for attitude determination. Payload pointing capability of better than 5 degrees can be accomplished using one magnetometer, one small pitch momentum wheel, and a simple B-dot control law operating on both the magnetometer measurements and an on-board local field reference model. Furthermore, as a natural consequence of B-dot control the pointing performance is insensitive to magnetometer biases. The operational altitude limitation is reached once the de-stabilizing gravity gradient torque exceeds the stabilizing aerodynamic torque, which can occur at altitudes beyond about 500 km, depending on solar panel deployment angles and local air density. Bus magnetic balancing using NASA Goddard's Spacecraft Magnetic Test Facility, which is critical for maximizing pointing performance, was also discussed in this paper. For the NRL space dart configuration, we were able to achieve a static (powered loads off) and dynamic (powered loads on) residual spacecraft dipole of less than 10 mA-$m^2$.

## REFERENCES

1. CubeSat Community Website, http://cubesat.atl.calpoly.edu/
2. AMSAT Cubesat Information, http://www.amsat.org/amsat-new/satellites/cubesats.php
3. Chin, A., Coelho, R., Brooks, L., Nugent, R., and Puig-Suari, J., "Standardization Promotes Flexibility: A Review of CubeSats' Success," 6th Responsive Space Conference, Los Angeles, CA, April 28-May 1, 2008.
4. Nugent, R., Munakata, R., Chin, A., Coelho, R., and Puig-Suari, J., "The CubeSat: The Picosatellite Standard for Research and Education," AIAA Space 2008 Conference and Exposition, San Diego, CA, Sept. 9-11, 2008.
5. Flagg, S., Bleier, T., Dunson, C., Doering, J., DeMartini, L., Clarke, P., Franklin, L., Seelbach, J., Flagg, J., Klenk, M., Safradin, V., Cutler, J., Lorenz, A., and Tapio, E., "Using Nanosats as a Proof of Concept for Space Science Missions: QuakeSat as an Operational Example," 18th Annual AIAA/USU Conference on Small Satellites, Logan, UT, Aug. 9-12, 2004.
6. Ubbels, W., Bonnema, A., van Breukelen, E., Doorn, J., van den Eikhoff, R., van der Linden, E., Aalbers, G., Rotteveel, J., Hamann, R., and Verhoeven, C., "Delfi-C3: A Student Nanosatellite as a Testbed for Thin Film Solar Cells and Wireless Onboard Communication," Proceedings of the 2nd International Conference on Recent Advances in Space Technologies, Istanbul, Turkey, June 9-11, 2005.
7. Lee, E., D'Ortenzio, M., Spremo, S., and Jaroux, B., "The *.Sat CubeSat Bus: When Three Cubes Meet," 19th Annual AIAA/USU Conference on Small Satellites, Logan, UT, Aug. 8-11, 2005.
8. Sarda, K., Eagleson, S., Caillibot, E., Grant, C., Kekez, D., Pranajaya, F., and Zee, R., "Canadian Advanced Nanospace Experiment 2: Scientific and Technological Innovation on a Three-Kilogram Satellite," Acta Astronautica, Vol. 59, 2006, pp. 236-245.
9. Nason, I., Puig-Suari, J., and Twiggs, R., "Development of a Family of Picosatellite Deployers Based on the CubeSat Standard," Proceedings of the IEEE Aerospace Conference, Big Sky, MT, March 9-16, 2002.
10. Hughes, P., Spacecraft Attitude Dynamics, John Wiley & Sons, 1986.